Research Article | Vol. 25, No. 5 | 6 Mar 2017 | OPTICS EXPRESS 5772

Optics EXPRESS

Dielectric lens guides in-plane propagation of surface plasmon polaritons

WEN-BO SHI, TIAN-YONG CHEN, HAO JING, RU-WEN PENG,* AND MU WANG

National Laboratory of Solid State Microstructures, School of Physics, and Collaborative Innovation Center of Advanced Microstructures, Nanjing University, Nanjing 210093, China
rwpeng@nju.edu.cn

Abstract: In this work, we present in-plane propagation of surface plasmon polaritons (SPPs) guided by a single dielectric (Al_2O_3) subwavelength lens. By mounting a designed Al_2O_3 nanoparticle on the silver film, the effective index of a silver-Al_2O_3 interface is influenced by the particle thickness, then the phase difference between the silver-air and silver-Al_2O_3 interface can be utilized to modulate the in-plane propagation of SPPs. We show that an elliptical Al_2O_3 lens transforms the diffusive SPPs into a collimated beam, whose direction of propagation and beam width can be easily controlled. We also present that a triangular Al_2O_3 lens significantly reforms the SPPs to a Bessel beam, which possesses non-diffractive and self-healing properties. Our investigation provides unique way to guide the in-plane transport of SPPs by using dielectric subwavelength elements, which may achieve potential applications in plasmonic integrated circuits.

OCIS codes: (250.5403) Plasmonics; (310.6628) Subwavelength structures, nanostructures; (130.3120) Integrated optics devices; (130.2790) Guided waves

References and links

1. K. C. Y. Huang, M. K. Seo, T. Sarmiento, Y. J. Huo, J. S. Harris, and M. L. Brongersma, "Electrically driven subwavelength optical nanocircuits," Nat. Photonics **8**(3), 244–249 (2014).
2. J. Wang, C. Hu, and J. Zhang, "Multifunctional and multi-output plasmonic meta-elements for integrated optical circuits," Opt. Express **22**(19), 22753–22762 (2014).
3. Y. Yang, Q. Li, and M. Qiu, "Broadband nanophotonic wireless links and networks using on-chip integrated plasmonic antennas," Sci. Rep. **6**, 19490 (2016).
4. H. Raether, *Surface Plasmons on Smooth and Rough Surfaces and on Grating* (Springer, 1988).
5. S. Maier, *Plasmonics: Fundamentals and Applications* (Springer, 2007).
6. W. L. Barnes, A. Dereux, and T. W. Ebbesen, "Surface plasmon subwavelength optics," Nature **424**(6950), 824–830 (2003).
7. E. Ozbay, "Plasmonics: merging photonics and electronics at nanoscale dimensions," Science **311**(5758), 189–193 (2006).
8. Y. J. Bao, B. Zhang, Z. Wu, J. W. Si, M. Wang, R. W. Peng, X. Lu, J. Shao, Z. F. Li, X. P. Hao, and N.-B. Ming, "Surface-plasmon-enhanced transmission through metallic film perforated with fractal -featured aperture array," Appl. Phys. Lett. **90**(25), 251914 (2007).
9. Z. J. Zhang, R. W. Peng, Z. Wang, F. Gao, X. R. Huang, W. H. Sun, Q. J. Wang, and M. Wang, "Plasmonic antenna array at optical frequency made by nano-apertures," Appl. Phys. Lett. **93**(17), 171110 (2008).
10. M. L. Brongersma and V. M. Shalaev, "Applied physics. The case for plasmonics," Science **328**(5977), 440–441 (2010).
11. W. Cai, W. Shin, S. Fan, and M. L. Brongersma, "Elements for plasmonic nanocircuits with three-dimensional slot waveguides," Adv. Mater. **22**(45), 5120–5124 (2010).
12. Q. Hu, D. H. Xu, Y. Zhou, R. W. Peng, R. H. Fan, N. X. Fang, Q. J. Wang, X. R. Huang, and M. Wang, "Position-sensitive spectral splitting with a plasmonic nanowire on silicon chip," Sci. Rep. **3**, 3095 (2013).
13. L. Yin, V. K. Vlasko-Vlasov, J. Pearson, J. M. Hiller, J. Hua, U. Welp, D. E. Brown, and C. W. Kimball, "Subwavelength focusing and guiding of surface plasmons," Nano Lett. **5**(7), 1399–1402 (2005).
14. A. B. Evlyukhin, S. I. Bozhevolnyi, A. L. Stepanov, R. Kiyan, C. Reinhardt, S. Passinger, and B. N. Chichkov, "Focusing and directing of surface plasmon polaritons by curved chains of nanoparticles," Opt. Express **15**(25), 16667–16680 (2007).
15. R. F. Oulton, V. J. Sorger, D. A. Genov, D. F. P. Pile, and X. Zhang, "A hybrid plasmonic waveguide for subwavelength confinement and long-range propagation," Nat. Photonics **2**(8), 496–500 (2008).
16. Q. Wang, X. Yuan, P. Tan, and D. Zhang, "Phase modulation of surface plasmon polaritons by surface relief

#285402 https://doi.org/10.1364/OE.25.005772
Journal © 2017 Received 24 Jan 2017; revised 1 Mar 2017; accepted 1 Mar 2017; published 2 Mar 2017

Optics EXPRESS

dielectric structures," Opt. Express **16**(23), 19271–19276 (2008).
17. H. Kim, J. Park, S. W. Cho, S. Y. Lee, M. Kang, and B. Lee, "Synthesis and dynamic switching of surface plasmon vortices with plasmonic vortex lens," Nano Lett. **10**(2), 529–536 (2010).
18. H. Wei, Z. Wang, X. Tian, M. Käll, and H. Xu, "Cascaded logic gates in nanophotonic plasmon networks," Nat. Commun. **2**, 387 (2011).
19. T. Matsui, T. Nomura, A. Miura, H. Fujikawa, N. Ikeda, D. Tsuya, H. T. Miyazaki, Y. Sugimoto, M. Ozaki, M. Hangyo, and K. Asakawa, "Wavefront control by stacked metal-dielectric hole array with variable hole shapes," Opt. Express **21**(5), 6153–6161 (2013).
20. D. H. Xu, K. Zhang, M. R. Shao, H. W. Wu, R. H. Fan, R. W. Peng, and M. Wang, "Band modulation and in-plane propagation of surface plasmons in composite nanostructures," Opt. Express **22**(21), 25700–25709 (2014).
21. Z. Li, J. Hao, L. Huang, H. Li, H. Xu, Y. Sun, and N. Dai, "Manipulating the wavefront of light by plasmonic metasurfaces operating in high order modes," Opt. Express **24**(8), 8788–8796 (2016).
22. M. U. González, A. L. Stepanov, J. C. Weeber, A. Hohenau, A. Dereux, R. Quidant, and J. R. Krenn, "Analysis of the angular acceptance of surface plasmon Bragg mirrors," Opt. Lett. **32**(18), 2704–2706 (2007).
23. S. Randhawa, M. U. González, J. Renger, S. Enoch, and R. Quidant, "Design and properties of dielectric surface plasmon Bragg mirrors," Opt. Express **18**(14), 14496–14510 (2010).
24. S. Griesing, A. Englisch, and U. Hartmann, "Refractive and reflective behavior of polymer prisms used for surface plasmon guidance," Opt. Lett. **33**(6), 575–577 (2008).
25. L. Feng, K. A. Tetz, B. Slutsky, V. Lomakin, and Y. Fainman, "Fourier plasmonics: Diffractive focusing of inplane surface plasmon polariton waves," Appl. Phys. Lett. **91**(8), 081101 (2007).
26. J. M. Steele, Z. Liu, Y. Wang, and X. Zhang, "Resonant and non-resonant generation and focusing of surface plasmons with circular gratings," Opt. Express **14**(12), 5664–5670 (2006).
27. I. P. Radko, S. I. Bozhevolnyi, A. B. Evlyukhin, and A. Boltasseva, "Surface plasmon polariton beam focusing with parabolic nanoparticle chains," Opt. Express **15**(11), 6576–6582 (2007).
28. A. Yanai and U. Levy, "Plasmonic focusing with a coaxial structure illuminated by radially polarized light," Opt. Express **17**(2), 924–932 (2009).
29. H. Sakai, S. Okahisa, Y. Nakayama, K. Nakayama, M. Fukuhara, Y. Ishii, and M. Fukuda, "Plasmonic integrated circuit operating with coherent plasmonic signals," in *Asia Communications and Photonics Conference* (OSA, 2015), paper ASu1D.4.
30. A. Arbabi, Y. Horie, M. Bagheri, and A. Faraon, "Dielectric metasurfaces for complete control of phase and polarization with subwavelength spatial resolution and high transmission," Nat. Nanotechnol. **10**(11), 937–943 (2015).
31. M. Khorasaninejad, W. T. Chen, R. C. Devlin, J. Oh, A. Y. Zhu, and F. Capasso, "Metalenses at visible wavelengths: Diffraction-limited focusing and subwavelength resolution imaging," Science **352**(6290), 1190–1194 (2016).
32. A. Hohenau, J. R. Krenn, A. L. Stepanov, A. Drezet, H. Ditlbacher, B. Steinberger, A. Leitner, and F. R. Aussenegg, "Dielectric optical elements for surface plasmons," Opt. Lett. **30**(8), 893–895 (2005).
33. E. A. Bezus, L. L. Doskolovich, and N. L. Kazanskiy, "Scattering suppression in plasmonic optics using a simple two-layer dielectric structure," Appl. Phys. Lett. **98**(22), 221108 (2011).
34. T. Zentgraf, Y. Liu, M. H. Mikkelsen, J. Valentine, and X. Zhang, "Plasmonic Luneburg and Eaton lenses," Nat. Nanotechnol. **6**(3), 151–155 (2011).
35. K. Lee, S. Y. Lee, J. Jung, and B. Lee, "Plasmonic achromatic doublet lens," Opt. Express **23**(5), 5800–5808 (2015).
36. Q. Zhan, "Evanescent Bessel beam generation via surface plasmon resonance excitation by a radially polarized beam," Opt. Lett. **31**(11), 1726–1728 (2006).

1. Introduction

Plasmonic integrated systems have great potentials in small scale integration, fast and sensitive detection, so there are many ongoing research efforts to realize nanoscale plasmonic circuits capable of manipulating light below the diffraction limit [1–3]. Surface plasmon polaritons (SPPs) arise from the coupling between electromagnetic waves and oscillations of conduction electrons at interface between a metal and a dielectric [4,5]. These are confined to sub-wavelength scale with notable field enhancement [6–8] and can be of use in multiple electronic and photonic applications [9–12]. To realize integrated plasmonic systems, plasmonic elements that can manipulate SPPs in-plane are particularly needed [13–21]. Subwavelength functional elements such as Bragg mirrors [22,23], prisms [24] and Fresnel zone plates [25] have been designed to address the requirements. Although most attempts focus on the development of highly confined SPPs [26–28], different methods that can control the propagation of SPPs on extended metallic surfaces are crucial for realizing plasmonic integrated circuits [11, 29].

Optics EXPRESS

Previously, modulation of SPPs was mostly carried out by using metallic elements such as nanoparticles [7], nanowires [12], or plasmonic metasurfaces [21], which led to additional energy loss. Recently, all dielectric element designs have been proposed for phase or polarization control in subwavelength scale [30,31]. Dielectric structures mounted on metals surface have proven to be an efficient method for the modulation of SPPs [32,33]. Dielectric arrays have been designed to realize phase modulation [16]. However, a single dielectric element designed as a modulator exhibits more flexibility. For example, plasmonic Luneberg and Eaton lenses have been demonstrated, and it has been shown that arbitrary refractive indices can be engineered by tuning the thickness of dielectric layer [34]. Plasmonic achromatic doublet lens made of materials with different dispersions have been designed to achieve broadband focusing [35]. However, functions beyond confinement of SPPs are rarely considered. Efforts can be undertaken toward manipulating SPPs by dielectric elements for realizing further applications in plasmonic integrated systems.

In this work, we analyze the manipulation of SPP propagation using a full dielectric Al_2O_3 lens. When an Al_2O_3 structure is mounted on a silver surface, the effective indices of the silver-air and silver-Al_2O_3 surfaces are different, providing a phase difference for the propagation of SPPs. We first analyze the effective index of the Al_2O_3 lens by changing its thickness and obtain the relationship between effective index and the lens thickness, which can be flexibly utilized in manipulating SPPs. Many previous works on plasmonic lenses focus on the confinement of SPPs, however, controlling the propagation is also significant for integrated plasmonic circuits. For example, a common way to excite SPPs is by using a laser beam focused on a slit in a metal surface; the SPP generated thus spreads in the form of a Gaussian beam that diffuses in all directions with a rapidly decreasing intensity. In this work, we propose a scheme to modulate SPPs into a collimated beam by using an Al_2O_3 elliptical lens. The direction of propagation and the width of the collimated beam can be controlled easily. Furthermore, we can modulate SPPs into a Bessel beam, the non-diffractive and self-healing properties of which are significant in plasmonic applications. We believe that our research will inspire more designs and applications on plasmonic integrated circuits.

2. Principle of the dielectric Al_2O_3 lens

The in-plane wave vector of SPPs excited in the metal and dielectric interface can be described as: $k_{SPP} = k_0(\varepsilon_d\varepsilon_m / \varepsilon_d + \varepsilon_m)^{1/2}$, where k_0 is the wave vector of incident light, ε_d is the permittivity of the dielectric and ε_m is the permittivity of the metal. We can use the expression $n_{eff} = \mathrm{Re}(\varepsilon_d\varepsilon_m / \varepsilon_d + \varepsilon_m)^{1/2}$ to represent the effective refractive index. Obviously, at different metal-dielectric interfaces, the effective refractive indexes are different. In this work, we try to use this feature to modulate the propagation of SPPs by placing an Al_2O_3 nanostructure in the silver film, where there exist two types of interfaces, *i.e.*, the Ag-air interface with effective refractive index n_1 and the Ag-Al_2O_3 interface with effective refractive index n_2. It is known that with the hyperbolic shape, elliptical lens can efficiently modulate the wave front of SPPs to affect the propagation, and some elliptical structures have been utilized in plasmonic systems [33, 35]. Here we try to design an elliptical Al_2O_3 nanoparticle as a lens in order to guide the in-plane propagation of SPPs. Figures 1(a) and (b) show the schematic view of the designed structure. A 100nm-thick silver film is grown on a glass substrate, and then a slit is etched on the silver film to generate the SPPs when a laser beam shines. On the propagation path of the SPPs, we place an elliptical lens made of Al_2O_3 with the thickness t, the width a and the height b. The lens locates at a distance of l from the slit. When SPPs propagate in the system, the phase difference is generated if the SPPs go through the same distance d in the Ag-air area as that in the Ag-Al_2O_3 area, which satisfies $\Delta\phi = (n_2 - n_1)\cdot d$. Thereafter, the equiphase surface of the SPPs excited by a plane wave source is changed from a plane to a converging sphere when the SPP passes through the elliptical Al_2O_3 lens. The SPPs can thus be focused by Al_2O_3 lens mounted on silver film, and

Optics EXPRESS

the focal length of lens is affected significantly by the difference of the effective refractive indexes of two types of interfaces. With increasing the effective refractive index n_2, the focal length becomes shorter, and the SPPs are focused closer to the lens.

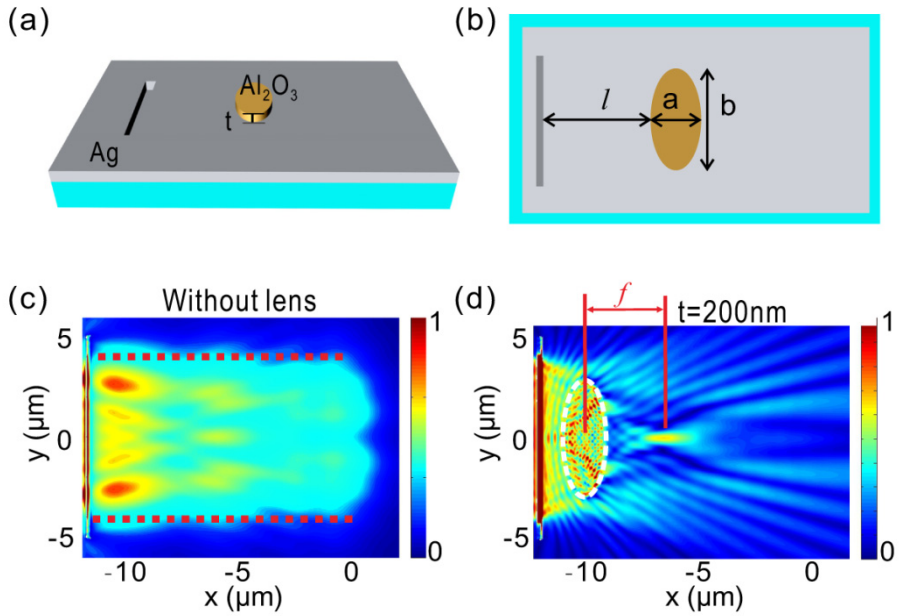

Fig. 1. (a) Schematic view of the designed elliptical lens on the silver film. The silver is 100 nm thick and covers the SiO_2 substrate. A slit is etched on the silver film to excite SPPs, and the Al_2O_3 elliptical lens is placed on the propagation path of the SPPs. The thickness of Al_2O_3 is t. (b) Top view of the structure. The width and height of lens are a and b, and the distance from lens to slit is l. (c) Calculated electric field distributions of SPPs generated by a plane wave source when there is no any lens in the system. (d) Calculated electric field distributions of SPPs generated by a plane wave source when there exists an elliptical Al_2O_3 lens in the system. The width and height of lens are a = 2μm and b = 6μm, the thickness is t = 200nm, and the distance from lens to slit is l = 1μm. The SPPs are focused by the lens and the focal length is f.

Now we show the focal effect of elliptical Al_3O_2 lens based on numerical calculations. We apply the finite-difference time-domain (FDTD) method by using commercial software (Lumerical FDTD Solution 8.0.1) to calculate the propagation of SPPs in the silver-air interface with or without the Al_3O_2 lens. The excitation source is placed above the slits with transverse magnetic (TM) polarization to excite SPPs. The wavelength of the source is set to 600nm. The permittivity of silver is $\varepsilon = -13.94 + 0.93i$, and the permittivity of Al_3O_2 is $\varepsilon = 3.12$ at the wavelength of 600nm. The loss in this system is included in calculations. The mesh in calculations is set as 2.5 nm. We set a 3D Frequency-domain field, and a power detector is used to obtain the electric field intensity at each point on the silver-air interface. In Fig. 1(c), we show the propagation of SPPs without any lens. The SPPs are excited by a plane wave source and they propagate as a decayed plane wave. However, once an elliptical Al_2O_3 lens, which has t = 200nm, a = 2μm, and b = 6μm, is put into the system, we can see that the SPPs are significantly focused by the elliptical lens with a focal length f, as shown in Fig. 1(d).

Optics EXPRESS

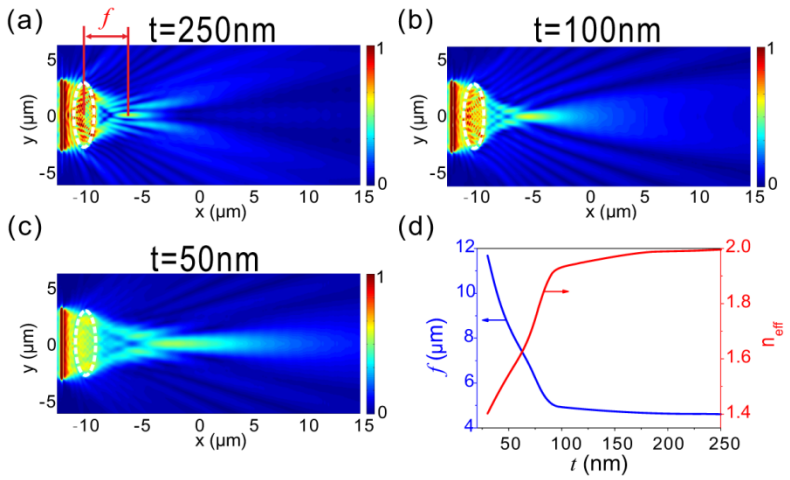

Fig. 2. (a) - (c) Calculated electric field distributions of focused SPPs for different thicknesses of Al_2O_3. The width and height of lens are a = 2μm and b = 6μm, and the distance from lens to slit is l = 1μm.The excitation source is a plane wave source of wavelength 600 nm. The focal length f clearly varies with change in thicknesses t. (d) Relationship of the thickness of Al_2O_3 t with focal length f (blue line) and effective index n_{eff} (red line) as derived from the calculation data.

Considering that the effective index of structure on the silver film is affected by its thickness, it is necessary to study how the focal length of Al_2O_3 lens is influenced by this thickness-dependent effective index. The focal length of the elliptical Al_2O_3 lens in this system is given by

$$f = \frac{n_{eff} r_1 r_2}{(n_{eff} - n_1)[n_{eff}(r_2 - r_1) + a(n_{eff} - n_1)]}. \quad (1)$$

where n_{eff} is the effective index of the Al_2O_3 area, and r_1 and r_2 are the effective radius of curvature of the left and right side of the lens, such that r_2 = - r_1. We use a plane wave source to generate the SPPs and focus the SPPs to a point to get the focal length f. For different thickness t, n_{eff} is different and the value of f changes as shown in Figs. 2(a)-2(c). Here we set a = 2μm, b = 6μm, l = 1μm and the wavelength of the source as 600nm. Electric field distributions shown in Figs. 2(a)-2(c) correspond to thickness t = 250nm, 100nm and 50nm, respectively. The value of f is measured directly from the field distributions. When t is large enough, n_{eff} is equal to n_2 ($n_2 \approx 2$ when wavelength is 600nm). By substituting these values in Eq. (1), we get r_1 = - r_2 = 8.4μm. Then for any given value of focal length f, we can obtain n_{eff} from Eq. (1). Thus by physically changing the thickness of Al_2O_3, we acquire the relationship between n_{eff} and t as shown in Fig. 2(d). We observe that when the thickness is larger enough, n_{eff} converges to n_2. When thickness is low (<100nm), n_{eff} decreases. In the latter condition n_{eff} is determined by both Al_2O_3 and air, and so it trends to n_1 as t decreases. That means by changing the thickness of Al_2O_3, the phase difference between the silver-air and silver- Al_2O_3 interface can be tuned; this result is useful in the phase modulation of SPPs.

3. Manipulation of SPP propagation using the designed lens

Here we try to modulate the propagation of SPPs by using an Al_2O_3 lens with t = 200nm. In most cases, SPPs are excited by a laser focused on a slit in a metal surface and they spread in the form of a Gaussian beam. Now we use a Gaussian wave source to excite the SPPs. As

Optics EXPRESS

shown in Fig. 3(b), the SPPs excited at the slits spread diffusively in front of the elliptical lens, and are transformed into a collimated beam after the lens. The diameter of the collimated beam is nearly unchanged during the propagation with high concentrated field. As a reference, we also calculate the electric field distribution of the SPP propagation without using the elliptical lens and find the SPPs spread around with intensity decrease quickly as shown in Fig. 3(a). By comparing Figs. 3(a) and 3(b), we observe that the elliptical lens we designed effectively changes the propagation of the SPPs and transforms the diffusive beam into a collimated beam.

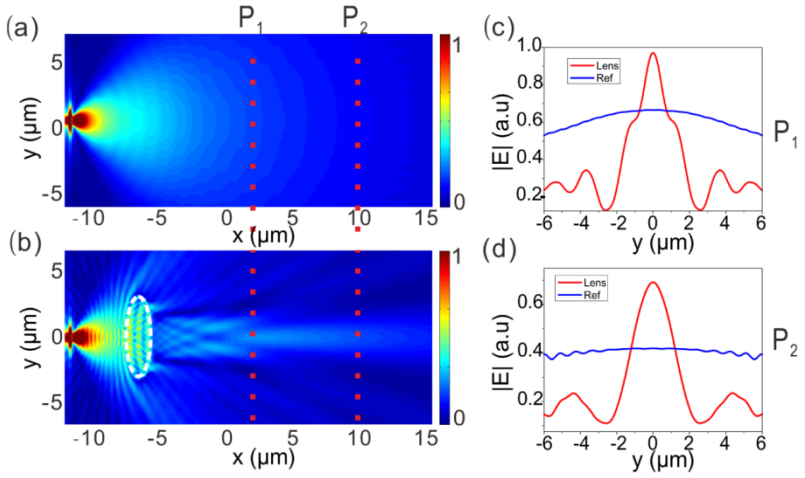

Fig. 3. (a) Calculated electric field distribution of propagation of SPPs without elliptical lens. (b) Calculated electric field distribution of the propagation of SPPs with elliptical lens. The parameters of elliptical lens are t = 200nm, a = 2μm and b = 6μm. A collimated beam is generated after the lens. (c) Density distributions at P1 (x = 2 μm) extracted from (a) and (b). (d) Density distributions at P2 (x = 10 μm) extracted from (a) and (b).

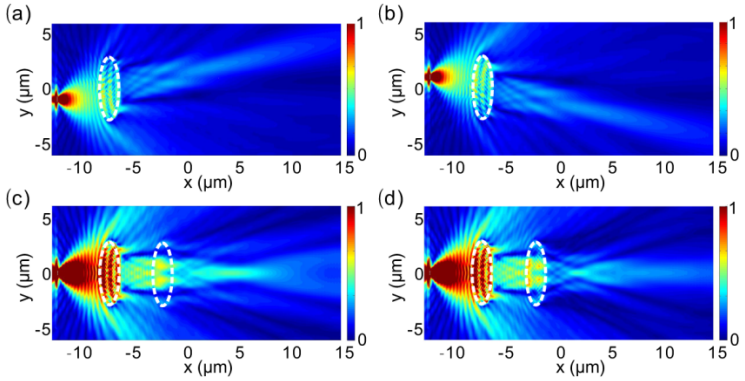

Fig. 4. Calculated electric field distributions (a) When the source is put downwards at y = −1μm. (b) When the source is put upwards at y = 1μm. (c) After adding another lens to focus the SPPs of thickness t = 50nm. (d) Adding another lens to focus the SPPs of thickness t = 80nm. The focus point can be tuned by changing the thickness.

To further investigate the differences of SPPs in these two conditions, we have extracted the intensity distributions at x = 2μm (P_1) and x = 10μm (P_2) shown in Figs. 3(c) and 3(d), respectively. We can see that, without the lens, the intensity of SPPs evenly distribute from y = −6 μm to 6 μm, while the intensity is restricted to y = −2 μm to 2 μm when the lens is present. The width of the collimated beam is nearly unchanged after long distance propagation as shown in Figs. 3(c) and 3(d). Moreover, the intensity of the collimated beam is

Optics EXPRESS

much larger than what is achieved without the lens, especially after long distance propagation as shown in Fig. 3(d). This implies that the energy of the SPPs is concentrated efficiently in the collimated beam, while slowing down the decay of the SPPs.

Next, we attempt to use the elliptical lens to manipulate the propagation of the SPPs. Take the propagation direction of SPPs for example. We show that when the source is moved downwards and the center is at y = –1 μm, the propagation direction of the collimated beam changes to a direction that is obliquely upwards as shown in Fig. 4(a). In contrast, when we place the source upwards at y = 1 μm, the collimated beam is tuned oblique downwards. In this procedure, the collimated beams keeps unchanged width and high concentrated field all the time, so the performance of the lens is very stable. That means the direction of propagation of the SPPs can be controlled using the elliptical lens simply by changing the relative position of the excitation point and the center of the elliptical lens. This property could be useful in plasmonic integrated systems for controlling the direction of propagation of the SPPs. Then we show that the collimated beam can be focused again if we add another elliptical lens as shown in Fig. 4. The refocused beam can be tuned by adjusting the thickness of the second lens. We repeat the process for different thicknesses of the second lens, specifically, t = 50 nm and t = 80 nm. We observe that the focus point and the size of focused point can be tuned with different thicknesses of the second lens as shown in Figs. 4(c) and 4(d). Figures 2(a)-2(c) show the focused SPPs by one elliptical lens, compare these figures with Fig. 4(d), we find that the refocused beam can be confined in smaller space, which implies that the elliptical lens can modulate SPPs into a highly confined region.

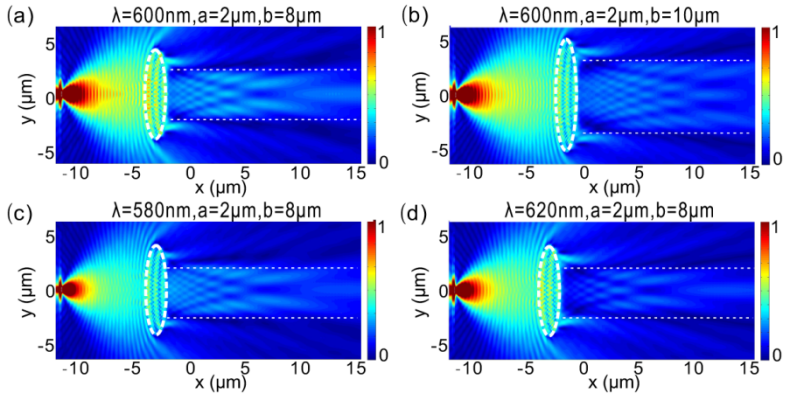

Fig. 5. Calculated electric field distributions when (a) Height of the elliptical lens is b = 8μm. (b) Height of the elliptical lens is b = 10μm. (c) Wavelength of excitation laser is 580nm. (c) Wavelength of excitation laser is 620nm. The straight dash lines mark the profiles of the collimated beams.

The shape of the lens is another factor influencing the modulation of SPPs. For example, if we set a = 2 μm, b = 8 μm, we observe from Fig. 5(a) that the focal length becomes larger and the width of the collimated beam increases. Comparing this with Fig. 5(b), where b = 10 μm, we find that by changing the value of b, the width of collimated beam is changed. We use straight dash lines to mark the profiles of the collimated beams and we can clearly find the widths are different in Figs. 5(a) and 5(b). So we can tune the width of the collimated beam by changing the height of the lens. We also consider the performance of the lens for different wavelengths. The results when the wavelength of excitation laser is 580 nm and 620 nm are shown in Figs. 5(c) and 5(d), respectively. We observe that the lens is capable of transforming SPPs to collimated beams in both these cases. By carrying out similar calculations at different wavelengths, we find that the elliptical lens with a = 2μm and b = 8μm can operate very well in the wavelength range from 580nm to 640nm. The bandwidth of such lens may be further broadened by tuning the shape of the lens and choosing more suitable metals in the system.

Optics EXPRESS

4. Manipulation of SPP into non-diffractive Bessel beam

Bessel beams do not suffer from diffractive spreading and are hence attracting a lot of research interest [36]. In this section, we consider the modulation of SPPs into a Bessel beam by using a triangular lens as shown in Fig. 6(a). We use the following parameter values for the triangular lens: a = 3 μm, b = 6 μm, t = 50 nm, and l = 8 μm. As shown in Fig. 6(b), we calculate the electric field distribution of the propagation of SPPs. We observe that the SPPs propagate through the triangular lens and become Bessel beams that have a central main lobe and several sub lobes on the sides. Even after propagating over a long distance, the main lobes show no diffraction. We have extracted the intensity distributions at x = 3 μm, 5 μm, and 8 μm; the results are shown in Fig. 6(c). We can see that the widths of the main lobe are nearly unchanged after long distance propagation, which exactly conforms to the non-diffractive properties of the Bessel beam.

Self-healing is another characteristic of Bessel beams. To confirm this feature, we introduce a defect in the forward path of the main lobe of the Bessel beam in the form of a circle etched on the silver film of diameter 2 μm. We observe from Fig. 6(d) that the main lobe of Bessel beam is destroyed when it encounters the circular defect. However, it exhibits self-healing after it propagates over a little distance. Although the intensity of main lobe decreases, it is still the strongest of all the lobes. Hence, we prove that the SPPs can be transformed into a Bessel beam using a triangular lens. The non-diffractive and self-heal Bessel beam of SPPs have great potential in applications related to optical and electric transport systems. Non-diffractive feature of Bessel beam is similar to that of collimated beam, while the self-healing feature of Bessel beam is quite unique and may be useful in plasmonic integrated systems.

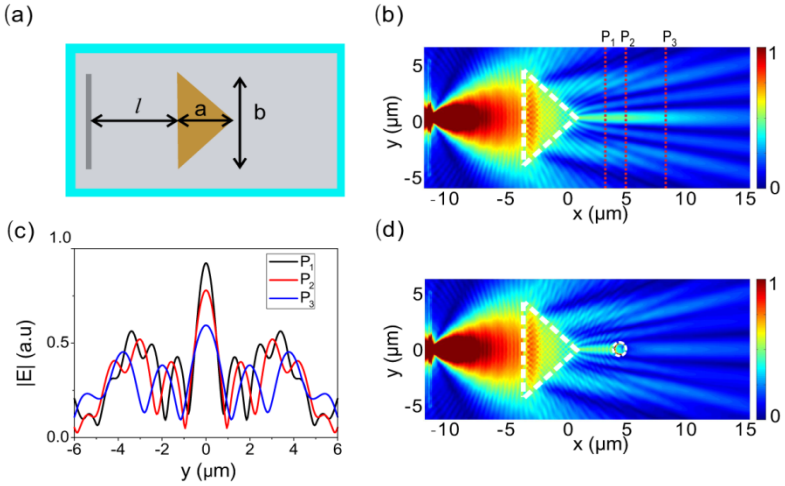

Fig. 6. (a) Top view of the structure with the triangular lens. (b) Calculated electric field distribution of the propagation of SPPs with the triangular lens with a = 3 μm, b = 6 μm, t = 50 nm, and l = 8 μm. (c) Intensity distributions at points P_1, P_2, P_3 shown in (b). (d) Calculated electric field distribution when a circular defect is added in the propagation path of the main lobe

5. Conclusion

In this study, we analyzed the effective index of Al_2O_3 structures of different thickness. We found that when the Al_2O_3 layer is very thin, the effective index at the metal-dielectric interface is determined by both Al_2O_3 and air, and it can be tuned by varying the thickness. We utilized this property to design lenses that are capable of manipulating the propagation of SPPs by reforming the SPPs into a collimated or Bessel beam. By designing an elliptical lens,

Optics EXPRESS

we transformed the SPPs from a diffused beam into a collimated beam, whose transmission direction and beam width can be varied by changing the lens construction parameters. The designed elliptical lens exhibited good performance over a broad range of frequencies from 580 nm to 620 nm. Moreover, we designed a triangular lens to transform the SPPs into a Bessel beam with non-diffractive and self-healing properties. By using the dielectric Al_2O_3 lens mounted on a silver film, we tuned the propagation of SPPs efficiently and brought out some interesting characteristics of SPP propagation. Our work is useful for 2D confined optical transport, and can potentially be applied in plasmonic integrated systems.

Funding

This work was supported by the National Natural Science Foundation of China (Grant Nos. 11634005, 61475070, 11474157, 11674155, and 11621091).